Operating conditions and stability of spin torque majority gates: Analytical understanding and numerical evidence

Adrien Vaysset, Mauricio Manfrini, Dmitri E. Nikonov, Sasikanth Manipatruni, Ian A. Young, Iuliana P. Radu, and Aaron Thean

Citation: J. Appl. Phys. **121**, 043902 (2017); doi: 10.1063/1.4974472
View online: http://dx.doi.org/10.1063/1.4974472
View Table of Contents: http://aip.scitation.org/toc/jap/121/4
Published by the American Institute of Physics

Operating conditions and stability of spin torque majority gates: Analytical understanding and numerical evidence

Adrien Vaysset,[1,a)] Mauricio Manfrini,[1] Dmitri E. Nikonov,[2] Sasikanth Manipatruni,[2] Ian A. Young,[2] Iuliana P. Radu,[1] and Aaron Thean[1,3]
[1]*IMEC, Leuven, Belgium*
[2]*Exploratory Integrated Circuits, Components Research, Intel Corp., Hillsboro, Oregon 97124, USA*
[3]*Department of Electrical and Computer Engineering, National University of Singapore, Singapore*

(Received 12 August 2016; accepted 8 January 2017; published online 23 January 2017)

The functionality of a cross-shaped Spin Torque Majority Gate (STMG) is primarily limited by the pinning of a domain wall (DW) at the center of the device. Here, an analytical model is built to calculate the conditions for such a pinning and to deduce the operating range. The assumptions of the model and the conclusions are validated by micromagnetic simulations. The total magnetic energy of the DW state is derived. By minimizing this energy with respect to two degrees of freedom, the DW stability condition is obtained. We find that the lateral length of the STMG is the critical dimension: it must be smaller than about five times the DW width. This result is confirmed by micromagnetic simulations with a high accuracy. In process, we solved a more fundamental problem: the macrospin limit of a finite ferromagnet containing one pinning site. We found the correction of the usual DW width expression due to finite length of wires. *Published by AIP Publishing.*
[http://dx.doi.org/10.1063/1.4974472]

I. INTRODUCTION

Scaling of both speed and density of Complementary Metal-Oxide Semiconductor (CMOS) field-effect transistor circuits to smaller characteristic sizes is becoming more and more challenging due to fundamental limits.[1] Among the possible complementary "beyond-CMOS" device options, a wide range of proposals use the properties of the electron spin or equivalently, magnetization, enabling the non-volatile logic. For example, in Nano-Magnetic Logic,[2–5] information is encoded in the magnetization and propagates between nanoscale magnets via dipolar coupling. Logic gates can also be built with Magnetic Tunnel Junctions[6,7] (MTJs). In a more disruptive approach, called Domain Wall (DW) logic,[8–11] the logic state propagates in one continuous ferromagnetic layer. These concepts should be more energy-efficient as they avoid multiple conversions between charge and spin computational variables.

One of the advantages of beyond-CMOS logic is that it does not have to be restricted to the standard NAND, NOR, and NOT gates. Instead, three-input majority gates[3,4,12–14] and NOT gates can be used as the building blocks of any arithmetic function.[15,16] Digital circuits would greatly benefit from this new computational paradigm as they would require fewer components and could be more compact.[16,17]

A three-input majority gate driven by Spin Transfer Torque[18,19] (STT) has been proposed in Ref. 13. It consists of a cross-shaped free layer shared between four Magnetic Tunnel Junctions (see Fig. 1). Variations of the Spin Torque Majority Gate (STMG) shape have been investigated,[20] but the "simple cross" remained the most reliable.

The binary information ("0" or "1") in the gate is represented by the magnetization orientation (up or down) in the free layer. Three MTJs write the input states via STT in a current perpendicular to plane configuration. The forth MTJ reads the output state via tunnel magnetoresistance. In principle, there is no in-plane current. The magnetic domains are mainly driven by the exchange interaction. As a consequence, the STMG works only at a very small size. The operating range has been extensively studied by micromagnetic simulations.[21] It was found that the device is limited by a main failure state consisting of a DW pinned at the center of the cross. Functionality is ensured if the parameter of the DW width, $\sqrt{A_{ex}/K_{eff}} > 1.21a$ (where A_{ex} is the exchange constant, K_{eff} is the effective anisotropy, and a is the arm width). Thus, it seems that the ratio of the DW width over the arm width a determines the working condition. However, that study did not include variations of the aspect ratio k, defined as the arm length over the arm width a (see Fig. 2). k was kept constant, equal to 7. Therefore, it is still unclear whether the limiting dimension is the arm width a or the arm length ka.

According to Ref. 21, the failure occurs when the DW state at the center of the cross is an energy minimum. Thus, the device operates properly when the DW state in the center is a saddle point of the energy landscape. In this article, we derive analytically the magnetic energy of a generalized domain wall state (Section II) and compare it against numerical simulations (Section III). Then, we seek the stationary points of the energy and deduce the DW stability conditions leading to failure of the STMG (Section IV). The operating condition is obtained for any aspect ratio k. These results allow to draw conclusions regarding the optimal aspect ratio of an STMG. Moreover, a fundamental problem is addressed through our analytical model: the macrospin limit of a finite ferromagnet containing one main pinning site. Operating conditions for a typical stack are given in Section V, and the limitations of the model are described in Section VI.

[a)]Also at Departement elektrotechniek (ESAT), KU Leuven, Leuven, Belgium.

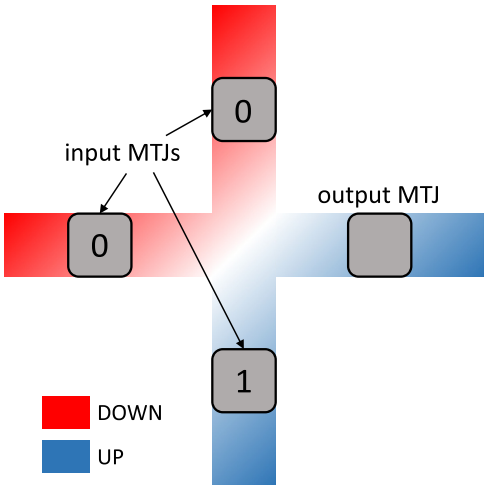

FIG. 1. Schematic representation of the spin-torque majority gate in the main failure state.

II. MODEL ASSUMPTIONS

A. Equivalent 1D model

The main failure state described in Ref. 21 is in fact degenerate. Depending on the two neighboring branches that are switched, the DW can be along one of the two diagonals at the center of the cross, and depending on the switching direction, there are also two possible domain orientations. This is a total of four energetically equivalent configurations. In the following, we assume without the loss of generality that the upper and left arms are in the UP state, while the lower and right arms are pointing DOWN (see Figure 2). The coordinate axes are rotated by 45°, as shown in Fig. 2(a), such that the DW lies in the yz-plane. m_z is positive when $x<0$ and negative when $x>0$.

DWs are commonly modeled in a wire infinitely extending in one dimension. Here, it cannot be considered as infinite since the size determines the failure or success. Therefore, the analytical expression of the energy must contain finite integral bounds.

According to the simulations performed in Ref. 21, magnetization variations with respect to y and z seem negligible in the failure state. As explained in the supplementary material, the energy density $\epsilon_{tot}(x,y,z)$ can then be expressed as a function of $\theta(x)$ where θ is the out-of-plane magnetization angle.

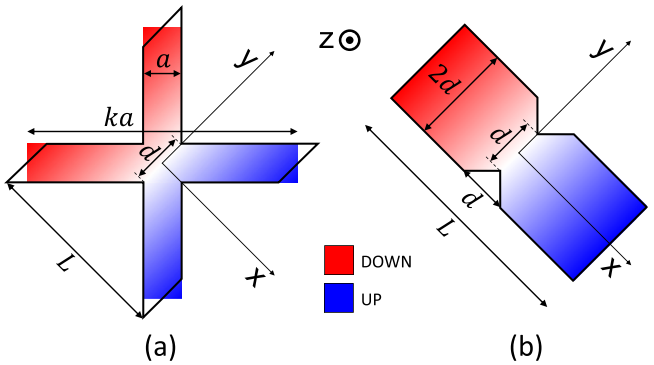

FIG. 2. Distribution of magnetization in a STMG and an equivalent ferromagnet. Red: magnetization up. Blue: magnetization down. Assuming beveled edges and a magnetization that varies only along x, the cross (a) is energetically equivalent to a rectangle with two notches (b).

For easier calculation of the energy integral, we modify the shape to have beveled the edges as illustrated in Fig. 2(a). Thus, the boundaries are located at fixed x and have fixed $\mathbf{m}$ values.

The total energy of this beveled cross (Fig. 2(a)) proves to be the same as the energy of a rectangle with two notches in the middle (Fig. 2(b)) (see supplementary material). This equivalence is useful to understand the possible equilibrium states. If a DW is energetically stable, its preferred position is between the two notches (i.e., at the center of the cross), which causes a failure. Therefore, the STMG is functional if a DW is unstable in the free layer, in other words, if the only equilibrium states are uniform (or "macrospin"). Thus, finding the operating range of the STMG amounts to answering a more fundamental question: what is the macrospin limit of a bounded ferromagnetic body containing one main pinning site? We refer here to the static macrospin limit. Dynamically, the reversal can be non-uniform, while the only stable states are macrospin.

The sizes of the two equivalent shapes are related by

$$L = \frac{ka}{\sqrt{2}}, \quad d = \sqrt{2}a. \tag{1}$$

The total energy can be expressed via the total magnetic energy density ϵ_{tot}

$$E_{tot} = \int_{-L/2}^{L/2} w(x)\, t\, \epsilon_{tot}(\theta(x))\, \mathrm{d}x, \tag{2}$$

where $w(x)$ is the width of the equivalent shape shown in Fig. 2(b). It is minimum at the center of the notch ($w=d$) and maximum outside the notch ($w=2d$).

B. Domain wall profile

To calculate the total energy, the angle of magnetization, $\theta(x)$, must be determined. In principle, it can be found by solving the Euler-Lagrange differential equation. Bruno[22] has solved it for a DW in a constriction, assuming an infinite wire. As mentioned previously, this assumption does not hold here.

Instead of solving the Euler-Lagrange equation, another approach[23,24] relies on finding a suitable analytic expression of the magnetization distribution as a function of one or more variable parameters. Then, the equilibrium state is obtained by minimizing the total energy with respect to these parameters.

The DW can either be Bloch (magnetization in the DW plane) or Néel (magnetization orthogonal to the DW plane). According to our micromagnetic simulations, they both have approximately the same energy. This is due to the specific cross shape that induces surface and volume magnetostatic charges for both types of wall. For convenience, the magnetization distribution of a Bloch configuration is considered here.

In the case of an infinite wire without constriction, the profile of a Bloch DW is

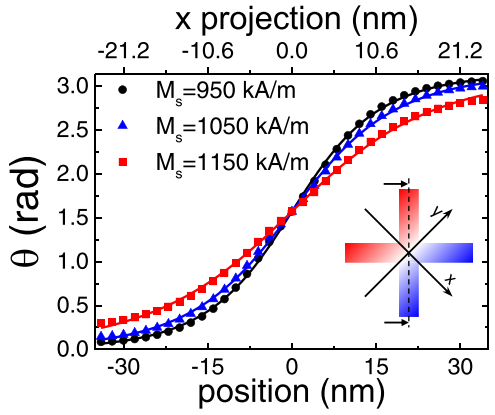

FIG. 3. Magnetization angle θ as a function of the position along the cross, as shown in the inset. The points are obtained from micromagnetic simulations. They are fitted with Eq. (3) (solid lines). The simulations were performed for a cross of $a = 10\,\text{nm}$ width, $L = 70\,\text{nm}$ length, $t = 1.2\,\text{nm}$ thickness, $K_s = 1\,\text{mJ/m}^2$ surface anisotropy. The red curve ($M_s = 1150\,\text{kA/m}$) is the limit case for DW stability: at $M_s = 1200\,\text{kA/m}$, the equilibrium state becomes uniform out-of-plane. As illustrated by the inset, the profile is not extracted perpendicularly to the DW, but at a 45° angle. The x coordinate (transverse to the wall) is shown on the top axis.

$$\theta(x) = 2\arctan\left(\exp\left(\frac{x - x_0}{\Delta}\right)\right) = \arccos\left(\tanh\left(\frac{x_0 - x}{\Delta}\right)\right), \tag{3}$$

where Δ is proportional to the wall width and x_0 is the position of the wall. Even though this expression was derived for a shape quite different from the cross, it fits very well with the DW profiles of our simulations,[25] as shown in Fig. 3. In this figure, $x_0 = 0$ and Δ is a fitting parameter. The quality of these fits gives enough confidence to use Equation (3) as an ansatz. The energy of the DW at equilibrium can then be calculated by minimization with respect to Δ and x_0, similarly to the methods used in Refs. 23 and 24.

III. DOMAIN WALL ENERGY: ANALYTICAL vs. NUMERICAL

Substituting Eq. (3) in Eq. (2) and using the expressions of the energy densities given in the supplementary material, one can calculate the three parts of the energy as a function of the geometrical parameters, the material parameters A_{ex}, K_s, and M_s, and the two degrees of freedom x_0 and Δ. The analytical expression of the total energy is then obtained

$$E_{tot} = E_{ex} + E_{anis} + E_{dip}, \tag{4}$$

where

$$E_{ex} = 2t A_{ex}\,\zeta, \tag{5a}$$

$$E_{anis} = 2t\,\frac{K_s}{t}\Delta^2\,\zeta, \tag{5b}$$

$$E_{dip} = 2t\left(-\frac{1}{2}\mu_0 M_s^2 (N_{zz} - N_{xx})\right)\Delta^2\,\zeta + 2t\,\frac{1}{2}\mu_0 M_s^2 N_{zz}\left(dL - \frac{d^2}{4}\right), \tag{5c}$$

where ζ is defined as

$$\zeta = \frac{3d}{\Delta} + \ln\left(\frac{1 + e^{\frac{2x_0}{\Delta}}}{e^{\frac{d}{\Delta}} + e^{\frac{2x_0}{\Delta}}}\right) + \ln\left(\frac{1 + e^{-\frac{2x_0}{\Delta}}}{e^{\frac{d}{\Delta}} + e^{-\frac{2x_0}{\Delta}}}\right) - \frac{2d}{\Delta}\left(\frac{e^{\frac{2x_0}{\Delta}}}{e^{\frac{L}{\Delta}} + e^{\frac{2x_0}{\Delta}}} + \frac{e^{-\frac{2x_0}{\Delta}}}{e^{\frac{L}{\Delta}} + e^{-\frac{2x_0}{\Delta}}}\right). \tag{6}$$

When the DW is located at the center of the cross ($x_0 = 0$), the exchange energy is

$$E_{ex} = 2t A_{ex}\,\zeta_0, \tag{7}$$

where ζ_0 is ζ in $x_0 = 0$ (see Eq. (6)). Namely,

$$\zeta_0 = \frac{3d}{\Delta} + 2\ln\left(\frac{2}{e^{\frac{d}{\Delta}} + 1}\right) - \frac{4d}{\Delta}\frac{1}{e^{\frac{L}{\Delta}} + 1}. \tag{8}$$

Since the anisotropy energy E_{anis} and the magnetostatic energy E_{dip} have similar expressions, one can define the effective anisotropy energy $E_{eff} = E_{anis} + E_{dip}$ which reads

$$E_{eff} = 2t\,K_{eff}\Delta^2\,\zeta_0 + 2t\,\frac{1}{2}\mu_0 M_s^2 N_{zz}\left(dL - \frac{d^2}{4}\right). \tag{9}$$

If Δ is known, E_{tot} can now be calculated analytically for a DW along the central diagonal ($x_0 = 0$). In order to validate the model, micromagnetic simulations are performed in the cross-shaped STMG, varying A_{ex} within a large range (from 2 to 80 pJ/m). When the equilibrium state is a DW, the fitting parameter Δ is extracted. In Fig. 4, the energies computed by the micromagnetic solver are plotted as a function of the extracted Δ. These simulation points are compared to the analytical results for the same range of Δ values. The agreement between the simulations and the analytical model is very good. The slight discrepancy observed at large Δ is mostly due to an overestimate of the exchange energy.

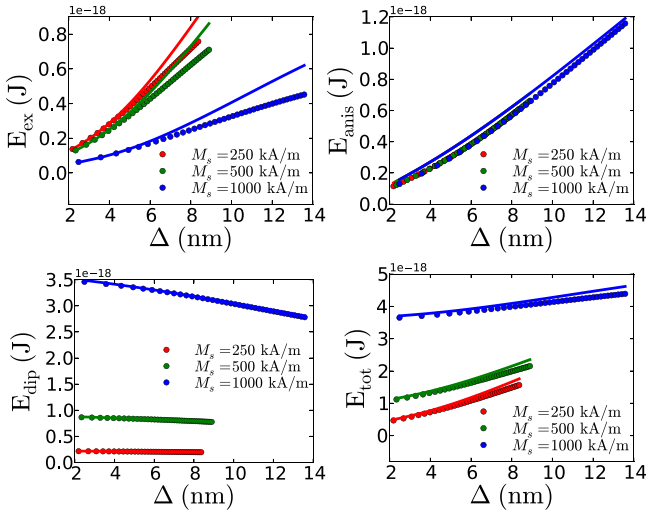

FIG. 4. Exchange energy E_{ex}, anisotropy energy E_{anis}, dipolar energy E_{dip}, and total energy E_{tot} as a function of Δ. Dots: micromagnetic simulations for $A_{ex} = 2 - 80\,\text{pJ/m}$, $M_s = 250, 500, 1000\,\text{kA/m}$, $a = 20\,\text{nm}$, $K_s = 1\,\text{mJ/m}^2$. Lines: energies predicted by the analytical model.

IV. OPERATING CONDITIONS

A. Stability conditions of the DW

By using the ansatz of Eq. (3), the energy landscape is reduced to only two degrees of freedom: x_0 and Δ. Since this model gives a realistic description of the DW at equilibrium, the true energy landscape can be approximated by Eqs. (4)–(6) in the vicinity of this equilibrium state.

The STMG works when the central DW is unstable and $K_{eff} > 0$. Therefore, we simply need to derive the DW stability condition at $x_0 = 0$ to deduce the operating conditions.

The DW is stable if it is an energy minimum, i.e., if it is a stationary point of E_{tot} and the eigenvalues of the Hessian matrix are positive. In $x_0 = 0$, the Hessian matrix $H(x_0, \Delta)$ is

$$H(0, \Delta) = \begin{pmatrix} \left.\frac{\partial^2 E_{tot}}{\partial x_0^2}\right|_{(0,\Delta)} & 0 \\ 0 & \left.\frac{\partial^2 E_{tot}}{\partial \Delta^2}\right|_{(0,\Delta)} \end{pmatrix}. \quad (10)$$

Therefore, the central DW is stable if there exists Δ_{eq} such that

(i) $\left.\frac{\partial E_{tot}}{\partial x_0}\right|_{(0,\Delta_{eq})} = 0,$

(ii) $\left.\frac{\partial E_{tot}}{\partial \Delta}\right|_{(0,\Delta_{eq})} = 0,$

(iii) $\left.\frac{\partial^2 E_{tot}}{\partial x_0^2}\right|_{(0,\Delta_{eq})} > 0,$

(iv) $\left.\frac{\partial^2 E_{tot}}{\partial \Delta^2}\right|_{(0,\Delta_{eq})} > 0.$

Δ_{eq} is the DW parameter at equilibrium. The condition (i) can be easily proven by differentiating E_{tot} (Eq. (4)) with respect to x_0. This is obvious, due to the symmetry of the cross. The condition (iv) is also trivial: if Δ_{eq} exists, $\left.\frac{\partial^2 E_{tot}}{\partial \Delta^2}\right|_{(0,\Delta_{eq})}$ is always positive. Sections IV B and IV C are dedicated to solving conditions (ii) and (iii). These solutions will be then gathered to obtain the operating condition.

B. Solution of condition (iii)

The second derivative of the total energy with respect to x_0 reads

$$\left.\frac{\partial^2 E_{tot}}{\partial x_0^2}\right|_{x_0=0} = 4t\left(\frac{A_{ex}}{\Delta^2} + K_{eff}\right)\kappa, \quad (11)$$

where

$$\kappa = \tanh^2\left(\frac{d}{2\Delta}\right) - \frac{2d}{\Delta}\frac{\tanh\left(\frac{L}{2\Delta}\right)}{\cosh^2\left(\frac{L}{2\Delta}\right)}. \quad (12)$$

In the out-of-plane case (i.e., $K_{eff} > 0$), the sign of $\left.\frac{\partial^2 E_{tot}}{\partial x_0^2}\right|_{x_0=0}$ is given by the sign of κ. The parameter κ determines the curvature of the energy well as a function of the device dimensions. When $\Delta \ll d$ (and thus $\Delta \ll L$), the curvature is maximum ($\kappa \to 1$). When $\Delta \gg d$, the curvature becomes negative, making the DW unstable. Since Eqs. (11) and (12) hold for any Δ value, they also hold for Δ_{eq}, addressing thus the condition (iii).

Unfortunately, in Eq. (12), it does not seem possible to separate Δ from the geometrical parameters d and L. However, substituting Eq. (1) in Eq. (12), κ can be written as a function of only two parameters: Δ/a and the aspect ratio k. We will see in Sec. IV C why this expression is particularly useful. In Fig. 5, κ is plotted (red curve) as a function of Δ_{eq}/a for three different aspect ratios k. The root Δ_{max}/a, is the upper bound for DW stability. As illustrated by the insets at the bottom of Fig. 5, if $\Delta_{eq} < \Delta_{max}$, the curvature of the energy landscape κ in $x = x_0$ is positive, which means that the DW state is a local energy minimum, while $\Delta_{eq} > \Delta_{max}$ leads to a negative curvature preventing the DW to be pinned at the center of the cross. The value of Δ_{max}, calculated numerically, is given in Table I. Δ_{max} can be

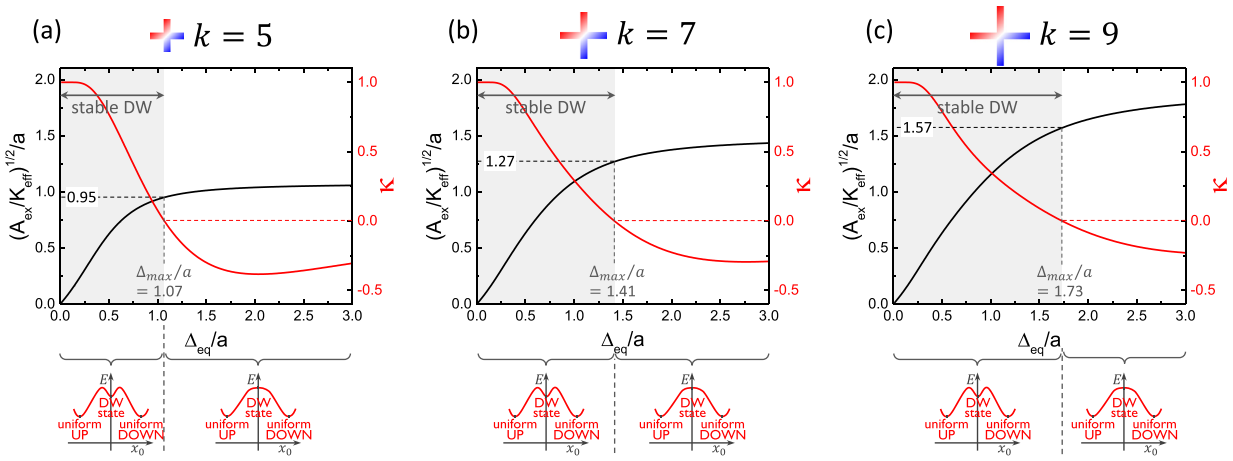

FIG. 5. DW stability conditions for the aspect ratios (a) $k = 3$ (short cross), (b) $k = 5$ (normal cross), and (c) $k = 7$ (long cross). In red: κ (y-axis on the right-hand side) as a function of Δ_{eq}/a. In black: $\sqrt{A_{ex}/K_{eff}}/a$ (y-axis on the left-hand side) as a function of Δ_{eq}/a. The DW is stable if $\kappa > 0$. The corresponding value of Δ_{eq}/a is 1.07 for the short cross, 1.41 for the normal cross, and 1.73 for the long cross. This limit value is reached when $\sqrt{A_{ex}/K_{eff}}/a$ is 0.95 (short cross) or 1.27 (normal cross) or 1.57 (long cross). Successful operation is expected outside the DW stability region, i.e., above the limit value of $\sqrt{A_{ex}/K_{eff}}/a$.

equivalently expressed as a function of the total cross length ka (last line of Table I). One can note that Δ_{max}/ka is almost constant. This is an interesting result that suggests that the DW becomes unstable when it is too wide to be contained within the total length of the cross ka. Since the STMG works when the DW is unstable, the total length of the cross must be as small as possible.

C. Solution of condition (ii)

The condition (iii) has been determined as a function of Δ_{eq} and the geometrical parameters k and a. At this stage, Δ_{eq}, the domain wall parameter at equilibrium is still unknown. To determine it, the condition (ii) must be solved. Differentiating E_{tot} (Eq. (4)) with respect to Δ yields

$$\left.\frac{\partial E_{tot}}{\partial \Delta}\right|_{x_0=0} = 2t\left[K_{eff}\Delta\,\xi_{eff} - \frac{A_{ex}}{\Delta}\,\xi_{ex}\right], \tag{13}$$

where

$$\xi_{ex} = 3\frac{d}{\Delta} - 2\frac{d}{\Delta}\frac{e^{d/\Delta}}{e^{d/\Delta}+1} - 4\frac{d}{\Delta}\frac{1}{e^{L/\Delta}+1} + \frac{dL}{\Delta^2}\frac{1}{\cosh^2\left(\frac{L}{2\Delta}\right)}, \tag{14}$$

$$\xi_{eff} = \frac{d}{\Delta}\tanh\left(\frac{d}{2\Delta}\right) + 2\frac{d}{\Delta}\tanh\left(\frac{L}{2\Delta}\right) - 4\ln\left(\cosh\left(\frac{d}{2\Delta}\right)\right) - \frac{dL}{\Delta^2}\frac{1}{\cosh^2\left(\frac{L}{2\Delta}\right)}. \tag{15}$$

The condition (ii), $\frac{\partial E_{tot}}{\partial \Delta}|_{x_0=0} = 0$, leads to

$$\Delta = \Delta_{eq} = \sqrt{\frac{A_{ex}}{K_{eff}}}\sqrt{\frac{\xi_{ex}}{\xi_{eff}}}. \tag{16}$$

Interestingly, the domain wall parameter Δ_{eq} is not equal to $\sqrt{\frac{A_{ex}}{K_{eff}}}$, its usual expression is valid for an infinite strip. Due to the boundaries and the pinning site, it is modified by the correction term $\sqrt{\frac{\xi_{ex}}{\xi_{eff}}}$. However, this expression is not particularly useful as ξ_{ex} and ξ_{eff} depend both on Δ. To find the solution, Eq. (16) must be rewritten as

$$\frac{\sqrt{A_{ex}/K_{eff}}}{a} = \frac{\Delta_{eq}}{a}\sqrt{\frac{\xi_{eff}}{\xi_{ex}}}. \tag{17}$$

Substituting Eq. (1) in Eqs. (14) and (15), ξ_{ex} and ξ_{eff} can be expressed as functions of Δ/a and k. Therefore, the term $\sqrt{A_{ex}/K_{eff}}/a$ in Eq. (17) is a function of only two parameters: Δ_{eq}/a and k. This result is similar to the solution of (iii) and can therefore be also plotted on Fig. 5 (black curve). These plots should not be misleading; we should keep in mind that, physically, the DW parameter at equilibrium Δ_{eq} is determined by the other parameters.

Interestingly, Δ_{eq} goes to infinity when $\frac{\sqrt{A_{ex}/K_{eff}}}{a}$ goes to $\frac{1}{2}\sqrt{\frac{k^3-1}{6k-3}}$. As a consequence, there is no Δ_{eq} when $\frac{\sqrt{A_{ex}/K_{eff}}}{a} \geq \frac{1}{2}\sqrt{\frac{k^3-1}{6k-3}}$, which means that the DW is not an equilibrium state and therefore that the STMG works in this case.

The approximation $\Delta_{eq} = \sqrt{A_{ex}/K}$ is commonly used through the literature, despite being only valid for an infinite wire. Here, the finite size and the pinning site lead to a different relation. When $\frac{\sqrt{A_{ex}/K_{eff}}}{a}$ is small (typically less than about 0.8), $\Delta_{eq} \approx 0.79\sqrt{A_{ex}/K_{eff}}$ and for large values of $\frac{\sqrt{A_{ex}/K_{eff}}}{a}$, Δ_{eq} decreases dramatically.

D. Summary

Since (i) and (iv) are trivial, the stability condition is obtained by combining (ii) and (iii). According to (iii), the DW is stable when $\Delta_{eq} < \Delta_{max}$. Plugging this into Eq. (17) for (ii) provides an upper bound for $\frac{\sqrt{A_{ex}/K_{eff}}}{a}$, as indicated in Fig. 5 (dashed black lines). This limit is the lower bound of operating conditions because the STMG works only when the DW is unstable. The lower bound is simply $K_{eff} = 0$. Equivalently, a maximum value of $\frac{\sqrt{A_{ex}/K_{eff}}}{ka}$ is determined. As shown in Table II, this ratio is almost constant with respect to k. Thus, the operating condition of the cross-shaped STMG is determined by two key parameters: $\sqrt{A_{ex}/K_{eff}}$ and ka (total length of the cross).

In simulations,[21] it was found that a cross of aspect ratio $k = 7$ works when $\frac{\sqrt{A_{ex}/K_{eff}}}{a} > 1.21$. The analytical model predicts 1.27, which is a very good agreement. This slight discrepancy can be explained. As mentioned in Ref. 21, if the domain wall is an energy minimum, it is likely to be pinned at the center. However, in the case of a very shallow minimum, it may not go through the pinning site since it does not follow exactly a quasi-static trajectory in the phase space. Recall that there is no in-plane current in STMG. The domain wall is first nucleated by the STT in the pillar areas. Then, the dynamics is mostly governed by the exchange interaction.

Practically, the patterning of the free layer is limited by the minimum printable width a. Since the correct operation is ensured only below a critical value of ka, the aspect ratio k must be as small as possible. Thus, a "short cross" is preferred. However, on such a cross, the inputs are very close to

TABLE I. Δ_{max} is the maximum value of Δ before the DW becomes unstable, according to (iii). a is the arm width. ka is the length of the cross.

	$k=5$	$k=7$	$k=9$
$\Delta_{max} =$	$1.07\,a$	$1.41\,a$	$1.73\,a$
$\Delta_{max} =$	$0.214\,ka$	$0.202\,ka$	$0.192\,ka$

TABLE II. The operating condition expressed as a function of a (arm width) and, equivalently, as a function of ka (total length of the cross).

	$k=5$	$k=7$	$k=9$
$\sqrt{\frac{A_{ex}}{K_{eff}}} >$	$0.95\,a$	$1.27\,a$	$1.57\,a$
$\sqrt{\frac{A_{ex}}{K_{eff}}} >$	$0.190\,ka$	$0.181\,ka$	$0.174\,ka$

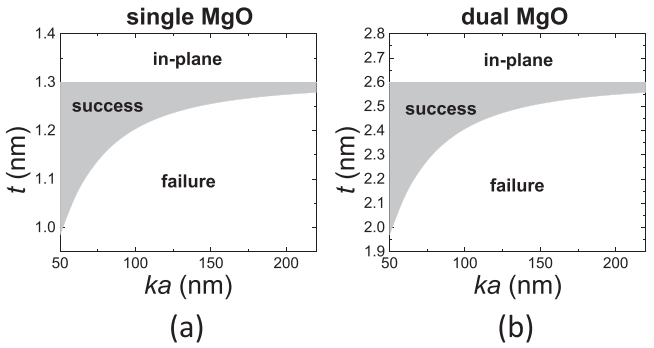

FIG. 6. Phase diagrams as a function of thickness and lateral length, for a CoFeB free layer in contact with one (a) and two (b) MgO interfaces. The parameters are $M_s = 1200\,\mathrm{kA/m}$, $A_{ex} = 2 \times 10^{-11}\,\mathrm{J/m}$, $N_{zz} - N_{xx} = 0.85$. In (a) $K_s = 1\,\mathrm{mJ/m^2}$. In (b) $K_s = 2\,\mathrm{mJ/m^2}$.

each other. The limiting factor for nanofabrication is then the inter-pillar distance.

V. DIMENSIONS-DEPENDENT PHASE DIAGRAM

The STMG comprises the same materials as an STT-Magnetic Random Access Memory (MRAM) stack. Therefore, in practice, the material parameters A_{ex}, M_s, K_s will be fixed. The thickness t and the length ka will be varied to reach the operating condition.

Replacing K_{eff} with $\frac{K_s}{t} - \frac{1}{2}\mu_0 M_s^2 (N_{zz} - N_{xx})$ in the operating condition (Table II) leads to

$$t > \frac{K_s}{\frac{A_{ex}}{(0.18\,ka)^2} + \frac{1}{2}\mu_0 M_s^2 (N_{zz} - N_{xx})}. \tag{18}$$

Neglecting the variation of $N_{zz} - N_{xx}$ with respect to t and ka, we obtain a simple condition on the thickness. Fixing the material parameters, the phase diagrams in Fig. 6 can be plotted as a function of t and ka.

For a typical single-MgO MTJ stack, if the lateral size ka is 50 nm, the thickness must be controlled by 3 Å ($1.0\,\mathrm{nm} < t < 1.3\,\mathrm{nm}$), while for $ka = 100\,\mathrm{nm}$, it must be controlled by 1 Å ($1.2\,\mathrm{nm} < t < 1.3\,\mathrm{nm}$). If a second MgO layer is inserted,[26] the interface anisotropy is potentially doubled and so is the allowed thickness range. Even though the model does not take roughness into account, the phase diagrams of Fig. 6 show that it is easier to obtain a well-functioning device for small ka and dual-MgO. The allowed thickness range is indeed wider.

VI. MODEL LIMITATIONS

In reality, the demagnetizing field is not uniform in the free layer. It is larger in the center than at the ends. Therefore, when K_s/t is small enough, the magnetization can be in-plane near the center and out-of-plane near the edge. This case was not observed in any of the simulations of Ref. 21 due to the small size. However, it can be observed at $a = 80\,\mathrm{nm}$, as shown in Fig. 7. In the range where correct operation is expected, the center becomes in-plane while the edge is still out-of-plane. As a consequence, the STMG cannot work in this case.

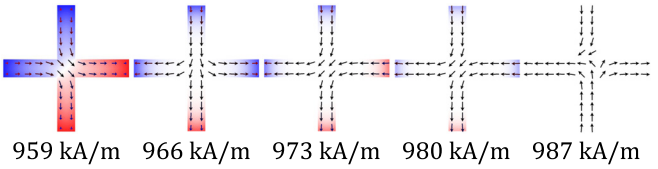

FIG. 7. Final states of STT simulations with the "C" input combination for different values of M_s (959–987 kA/m). The demagnetizing field increases as M_s increases, resulting in a transition from out-of-plane to in-plane magnetized ferromagnet. $a = 80\,\mathrm{nm}$, $K_s/t = 560\,\mathrm{kJ/m^3}$. Red: magnetization up. Blue: magnetization down.

This failure mode affects STMGs with a larger than about 60 nm. It is worth mentioning that it should not be an issue for future logic devices, since a must be much smaller than 60 nm to be competitive with CMOS logic as both will be manufactured by lithography with the smallest available feature size. However, it may make experimental proof of concept more challenging, since it will likely not use the cutting-edge lithography.

VII. CONCLUSION

In conclusion, an analytical model has been built to calculate the operating condition of the STMG for any aspect ratio k. The assumptions of the model have been compared against micromagnetic simulations and validated. Since the DW causes a failure, the device operates reliably when the only stable states are uniform. Thus, the STMG is functional if it can be only macrospin at equilibrium. It has been found that $\sqrt{A_{ex}/K_{eff}}$ must be larger than $\sim 0.18\,ka$. To put it another way, the lateral size must be smaller than about five times the DW width. This general result is valid for any aspect ratio k and is in a very good agreement with the micromagnetic simulations[21] for $k = 7$. In principle, K_{eff} can be easily decreased such that the working condition is fulfilled. However, we have demonstrated that, for a large size, the allowed thickness range is dramatically reduced. Consequently, the length of the cross is the limiting factor and must be reduced to obtain an experimental proof-of-concept.

To devise the STMG technology, key integration obstacles should be addressed. Extreme UV lithography is necessary to define sub-10 nm MTJs in very dense arrays. Additionally, the etching of these minute MTJs is very challenging but a recent report[27] sheds light to patterning feasibility of small tunnel junctions.

SUPPLEMENTARY MATERIAL

See supplementary material for the expressions of the energy terms and the proof of the shape equivalence.

[1]V. V. Zhirnov, R. K. Cavin, J. A. Hutchby, and G. I. Bourianoff, Proc. IEEE **91**, 1934 (2003).
[2]R. P. Cowburn and M. E. Welland, Science **287**, 1466 (2000).
[3]S. Breitkreutz, J. Kiermaier, I. Eichwald, X. Ju, G. Csaba, D. Schmitt-Landsiedel, and M. Becherer, IEEE Trans. Magn. **48**, 4336 (2012).
[4]I. Eichwald, S. Breitkreutz, G. Ziemys, G. Csaba, W. Porod, and M. Becherer, Nanotechnology **25**, 335202 (2014).
[5]M. T. Niemier, E. Varga, G. H. Bernstein, W. Porod, M. T. Alam, A. Dingler, A. Orlov, and X. S. Hu, IEEE Trans. Nanotechnol. **11**, 220 (2012).
[6]A. Ney, C. Pampuch, R. Koch, and K. H. Ploog, Nature **425**, 485 (2003).
[7]L. Leem and J. S. Harris, J. Appl. Phys. **105**, 07D102 (2009).

[8]D. A. Allwood, G. Xiong, C. C. Faulkner, D. Atkinson, D. Petit, and R. P. Cowburn, Science **309**, 1688 (2005).
[9]D. M. Bromberg, D. H. Morris, L. Pileggi, and J. G. Zhu, IEEE Trans. Magn. **48**, 3215 (2012).
[10]J. A. Currivan, Y. Jang, M. D. Mascaro, M. A. Baldo, and C. A. Ross, IEEE Magn. Lett. **3**, 3000104 (2012).
[11]K. Omari and T. Hayward, Phys. Rev. Appl. **2**, 044001 (2014).
[12]A. Imre, G. Csaba, L. Ji, A. Orlov, G. H. Bernstein, and W. Porod, Science **311**, 205 (2006).
[13]D. E. Nikonov, G. I. Bourianoff, and T. Ghani, IEEE Electron Device Lett. **32**, 1128 (2011).
[14]S. Klingler, P. Pirro, T. Brächer, B. Leven, B. Hillebrands, and A. V. Chumak, Appl. Phys. Lett. **105**, 152410 (2014).
[15]S. B. Akers, in *Symposium on Switching Circuit Theory and Logical Design (SWCT)* (IEEE, 1962), pp. 149–158.
[16]L. Amaru, P.-E. Gaillardon, and G. D. Micheli, IEEE Trans. Comput. Des. Integr. Circuits Syst. **35**, 806 (2016).
[17]L. Amaru, P.-E. Gaillardon, S. Mitra, and G. De Micheli, Proc. IEEE **103**, 2168 (2015).
[18]L. Berger, Phys. Rev. B **54**, 9353 (1996).
[19]J. Slonczewski, J. Magn. Magn. Mater. **159**, L1 (1996).
[20]D. E. Nikonov, S. Manipatruni, and I. A. Young, J. Appl. Phys. **115**, 17C736 (2014).
[21]A. Vaysset, M. Manfrini, D. E. Nikonov, S. Manipatruni, I. A. Young, G. Pourtois, I. P. Radu, and A. Thean, AIP Adv. **6**, 065304 (2016).
[22]P. Bruno, Phys. Rev. Lett. **83**, 2425 (1999).
[23]H.-D. Dietze and H. Thomas, Z. Phys. **163**, 523 (1961).
[24]A. Aharoni, J. Appl. Phys. **37**, 3271 (1966).
[25]The largest deviation between the fitting curves and the simulation data is near the edges. This difference can be explained by the micromagnetic boundary condition $\partial \mathbf{m}/\partial \mathbf{n} = 0$ not being satisfied by the general expression (3). A third parameter could be introduced in order to comply with the boundary conditions. However, it would greatly increase the complexity of the model without increasing significantly the accuracy.
[26]Z. Diao, A. Panchula, Y. Ding, M. Pakala, S. Wang, Z. Li, D. Apalkov, H. Nagai, A. Driskill-Smith, L. C. Wang, E. Chen, and Y. Huai, Appl. Phys. Lett. **90**, 132508 (2007).
[27]H. Sato, E. C. I. Enobio, M. Yamanouchi, S. Ikeda, S. Fukami, S. Kanai, F. Matsukura, and H. Ohno, Appl. Phys. Lett. **105**, 062403 (2014).